

1 **Title: The relationship between size, abundance, and mass of particles in the surface and bottom**
2 **waters of the Chesapeake Bay**

3

4 **Authors:**

5 **Emily C. Dougherty,**

6 **University of Maryland Center for Environmental Science, Horn Point Laboratory**

7 **emilydougherty14@gmail.com, 610-705-2489**

8 **Jacob A. Cram,**

9 **University of Maryland Center for Environmental Science, Horn Point Laboratory**

10 **jcram@umces.edu, 410-221-8481**

11 **Ashley Hollins**

12 **University of Maryland Center for Environmental Science, Horn Point Laboratory**

13 **ahollins@umces.edu**

14

15

16

17

18 **Acknowledgments**

19 The authors thank the MD Sea Grant REU program for supporting E.C.D during the sample collection

20 phase of this project, as well as University of Maryland Center for Environmental Science for

21 supplying J.A.C with start-up funds and ship time to complete this research. The authors thank M.

22 Reynolds for assistance in field collection, S. Malkin and C. Fuchsman for coordinating field sampling

23 efforts, L. Sanford for teaching us how to use the LISST and for helpful suggestions on analysis and

24 writing, as well as the captain and crew of the R.V. Rachael Carson.

25 **Abstract**

26 Particulate matter modulates the transport of carbon and nutrients through estuarine
27 environments. In the Chesapeake Bay, sinking of particles and their consumption by microbes likely
28 modulates the emergence of a seasonal oxygen deficient zone. The relationship between particle size
29 and abundance affects the transport dynamics of the particles and the biology of associated organisms.
30 The variability of particle characteristics has not previously been characterized across the length of the
31 Chesapeake Bay, nor has it been compared to the oxygen deficient zone. Therefore, we measured the
32 size to mass and size to abundance relationship of suspended particles along the Chesapeake Bay
33 during a major deoxygenation event. A laser scattering instrument measured particle size and
34 abundance at six stations. Five particle size classes were sampled at surface and bottom depths.
35 Particles in the less saline northern end of the Bay were less massive relative to size than particles
36 farther south. Estimates of total particle mass, calculated by combining particle size to mass and
37 particle size to abundance data, suggested that the anoxic region has lower particulate mass than
38 overlying oxic water, perhaps because stratified water above the oxygen minimum zone keeps particles
39 from the productive top layer from mixing into this region. Total particle mass was higher just above
40 the sediment, suggesting resuspension of benthic particles. Our data provide the first systematic survey
41 of size resolved particle abundances across the Chesapeake Bay oxygen minimum zone and provide
42 context to future work in evaluating the biogeochemical role of particles in this environment.

43
44 **Keywords: particles, particle size distribution, Chesapeake Bay, anoxia**

45
46
47
48

49 **Introduction**

50 Particulate Matter (PM) is comprised of both organic (Particulate Organic Matter -- POM) and
51 inorganic components and is an essential part of carbon transport in estuarine environments. Estuaries
52 facilitate and regulate the transport of PM, as well as dissolved carbon, from rivers into the oceans
53 (Fisher et al. 1998; Loh et al. 2006) and produce PM *in situ* (Savoie et al. 2011; Middelburg and
54 Herman 2007). The dynamic conditions of estuaries create gradients in the abundance and composition
55 of particles, which vary over spans of hours, seasons, or years (Canuel and Zimmerman 1999) and
56 between locations (Fisher et al. 1998).

57 The concentration, size distribution, and dynamics (including aggregation and disaggregation)
58 of PM in estuaries is affected by factors including turbulence, differential settling, Brownian motion,
59 salinity gradients, and compounds produced by organisms that cause particles to aggregate (Eisma et al.
60 1991). High collision frequency, which depends on the concentration of particles and the energy of the
61 water, can lead to particle aggregation, while turbulence breaks up particles (Fugate and Friedrichs
62 2003). Near the surface, particle size may be limited by low collision frequency (Fugate and Friedrichs
63 2003). Aggregation and breakup together drive particle size distributions to an equilibrium distribution,
64 which can vary regionally in response to variation in turbulence and other factors (Chen et al. 1994).
65 Sinking speed also affects particle size distributions, with denser faster sinking particles leaving the
66 pycnocline more quickly than less dense slowly sinking or non-sinking particles (Fugate and Friedrichs
67 2003). PM that reaches the lower water column of estuaries settles into the bed, where strong
68 turbulence may cause re-suspension of large particles and more breakup (Hill et al. 2001).

69 The Chesapeake Bay is the largest estuary in the United States, with the main stem measuring
70 320 km (Schubel and Pritchard, 1986). Within the Bay, there are strong salinity gradients, with a low
71 salinity region (< 0.5 ppt) in the northern section, a mesohaline zone (0.5 – 25 ppt) extending
72 approximately from 39°N latitude to the mouth of the Potomac River, and a high salinity region (> 25

73 ppt) near the mouth of the Bay (Maryland Department of the Environment). The Chesapeake Bay has
74 an expanding region of seasonal anoxia (Testa 2018; Kemp 1992), with deficits occurring annually in
75 the mesohaline region (Officer et al. 1984). Deoxygenation is driven by microbes at depth consuming
76 the organic portion of particles that originate in high production surface waters (Robinson 2019). In the
77 Chesapeake Bay, these particles originate from surface waters primarily in the mainstem of the Bay
78 (Wang and Hood 2021). Anoxic regions are intensified by sewage and agricultural runoff, which
79 increase the rate of phytoplankton production (Canuel and Zimmerman 1999).

80 Since the Chesapeake Bay is a region of high biological productivity and diverse habitats, there
81 is high variability in the origin and distribution of PM. The balance of aggregation, disaggregation, and
82 particle transport differ between the mouth of the Bay, the seasonally anoxic mesohaline, and the Upper
83 Bay. Several studies have characterized particle size distributions near the mouth of the Bay: One of
84 these studies combined acoustic and optical measurements of particle properties and identified
85 temporal variability in the sinking speed and size properties of particles near the mouth of the Bay
86 (Fugate and Friedrichs 2002). In another site in the lower Bay, it was found that higher turbulent kinetic
87 energy near the bed is associated with larger particle sizes (Fugate and Friedrichs 2003). This result
88 contrasted with other estuarine river environments in this study, where turbulence near the riverbed
89 fragments particles, keeping their sizes small. The authors suggested that the Chesapeake Bay has a
90 biologically active benthic community, which produce compounds that create large aggregate particles
91 under turbulent conditions (Fugate and Friedrichs 2003).

92 No study, to our knowledge, has characterized the particle size distribution spectrum in the
93 mesohaline region of the Bay. However, several studies have explored the origin of particles
94 contributing to the seasonally anoxic region of the Bay. Particle transport into the mesohaline is driven
95 in large part by advection of deep water from the high salinity mouth of the Bay and particle sinking
96 (Jonas 1992). Particle tracking experiments have shown that particles that ultimately sink into the

97 anoxic region of the Bay vary in their origin depending on the tidal cycles and corresponding currents
98 (Wang and Hood 2021). The organic portion of this particulate matter has been shown to degrade
99 quickly (Jonas and Tuttle 1990), and so fuels the oxygen removal in this anoxic region.

100 In the Upper Bay, there is a defined estuarine turbidity maximum (ETM) region, where the
101 Susquehanna River meets the more brackish waters of the main Bay (Schubel and Biggs 1969). The
102 ETM is caused by suspension and entrainment of sediment from the bay floor, which is maintained by
103 interactions between tidal forces and the steep salinity gradient (Sanford et al. 2001). This region is
104 characterized by vertical stratification and seasonal variability in particle concentrations (Fisher et al.
105 1998). Particle concentrations are influenced by particles coming from the Susquehanna River,
106 particularly in spring when there is more runoff into the river (Schubel and Biggs 1969). Total particle
107 concentrations in the upper Bay are generally higher than in the mesohaline region (Biggs 1969).

108 While each of these studies examined particle distributions at specific regions and sites in the
109 Chesapeake Bay, no previous study has, to our knowledge, characterized particle size distribution
110 across the length of the Bay. While comparing the different papers can give us insight about differences
111 between these regions, they each use different measurements and are taken at different times.
112 Furthermore, no study to our knowledge has examined particle size distributions within, around and
113 above the oxygen deficient zone. Therefore, in this study we carried out measurements of the particle
114 size to abundance distribution and size to mass distribution along the surface and bottom of the
115 mainstem of the Bay, from the high salinity mouth of the Bay to the lower salinity waters just below the
116 ETM. Such data will provide information about the processes that shape particle size and transport. In
117 particular, we are interested in how the anoxic zone affects particle dynamics, because particles
118 attenuate slowly in anoxic regions (Rasse and Dall’Olmo 2019). Exploring the interactions between
119 anoxic environments and particle size distributions has the potential to provide clues about how
120 hypoxia relates to the regional carbon cycle.

121 **Methods**

122 Samples and observations were collected July 22, 23, and 24, 2019, on the R/V *Rachel Carson*
123 from six stations along the main stem of the Chesapeake Bay, corresponding to the Maryland
124 Department of the Environment's water quality monitoring stations CB3.1 (39.24°N,76.24°W,
125 corresponding to 13.3m water column depth), CB3.2 (39.16°N, 76.30 °W, 12.2 m), CB3.3C (39.00°N,
126 76.36°W, 24.1 m), CB4.3C (38.56°N, 76.43°W, 27.1 m), CB5.1 (38.32°N, 76.29°W, 34.3 m), and
127 CB5.5 (37.69°N, 76.19°W, 17.7 m) (Fig. 1A).

128 A Seabird CTD (Conductivity, Temperature, and Depth), mounted on the CTD-rosette measured
129 water Temperature, Salinity, Fluorescence, and pH throughout the water column. At each station, a
130 laser *in-situ* scattering and transmissometry (LISST-100X) instrument (Sequoia Scientific, Inc.) was
131 lowered into the water to measure a vertical profile of the particle size distribution spectrum. The
132 LISST uses the laser light diffracted by particles to provide a reading of the total volume concentration
133 ($\mu\text{L Particles/L Water}$) of particles in several bins, each represented by a minimum particle diameter
134 (LISST 100X Manual 2015). Particles were assumed to be spherical in shape, so the diameters were
135 used to calculate the average volume of an individual particle in each bin. From the total volume
136 sampled and the individual particle volumes, the number of particles per liter of water was calculated
137 for each size bin. For purposes of comparison to particle mass measurements, the LISST size data were
138 grouped into the filter size fractions of 1.2 μm , 5 μm , 20 μm , 53 μm , and 180 μm , each corresponding
139 to our filter size fractions, by summing particle abundances of all LISST size bins that fell within each
140 filter size bin. No particle number was obtained for the 0.2 μm filter size, since this size is below the
141 LISST detection threshold of 1 μm . Similarly, LISST measurements were not recorded for the 500 μm
142 size fraction as we found measurements above 200 μm to be inconsistent. Initial data processing was
143 carried out by the proprietary LISST-SOP software provided for the LISST-100X by Sequoia scientific.

144 All subsequent data analysis was performed in the R statistical programming language (R Core Team
145 2019).

146 Water samples were collected in the surface mixed layer and five meters above the floor of the
147 Bay at each station. At station 4.3C a sample was also taken at the oxycline in the mid water column
148 (Fig. 1). For each sample, between 13 and 20 liters of water were collected with Niskin bottles and
149 gravity filtered, in sequence, through five nylon filters with diameters of 150 μm and decreasing pore
150 sizes of 500 μm , 180 μm , 53 μm , 20 μm , and 5 μm . Each filter was rinsed with 0.2 μm filtered
151 seawater from the same station. An aliquot of this rinse water was vacuum filtered through a pre-
152 weighed 25 mm diameter 1.2 μm pore size glass fiber filter (Whatman 16936209) and was saved for
153 analysis of particle mass.

154 In the lab, particle mass was measured for each size fraction by drying and re-weighing the pre-
155 weighed glass fiber filters and calculating its change in mass. This value was divided by the number of
156 particles corresponding to this size bin to find the average mass per particle in each size class.

157 The slope and intercept of the particle size to abundance relationship and size to mass
158 relationship were calculated on the log of the values of particle size, abundance and mass. The slope of
159 the size to abundance relationship is called the particle size distribution slope (Jackson et al. 1997), and
160 the slope of the size to mass relationship is the particle fractal dimension (Jackson et al. 1997).

161 Intercepts correspond to the predicted abundance and mass of 1 μm particles. Total particle mass
162 profiles throughout the water column were estimated by multiplying particle abundances in each size
163 class, measured by the LISST, by the empirically derived size to mass relationships determined by the
164 filtration method. Data from the top meter of the water column was removed from the plots for particle
165 mass and abundance profiles, as light from the surface is known to create artifactually high estimates of
166 particle abundance in these samples (L. Sanford pers. Comm.).

167

168 **Results**

169 *Physics and Chemistry of the Bay*

170 Stations followed a salinity gradient, with the lower salinity associated with northern stations
171 near the mouth of the Susquehanna River and higher salinity with stations closer to the mouth of the
172 Bay (Fig. 1A-B). While station 3.1 was fully mixed, all remaining stations had an oxygenated mixed
173 layer, followed by a pycnocline, below which water was cooler and more saline (Fig. 1B, C, F). All
174 stations except 3.1 and 5.5 were anoxic below the pycnocline. The deepest samples at station 4.3 and
175 5.1 were sulfidic, as evidenced by a sulfurous smell to the water (M. Gomes Pers. Comm.). Chlorophyll
176 fluorescence was present at all stations through the pycnocline (Fig. 1D). pH was lower in the two
177 upper-most stations than in the others (Fig. 1E).

178 *Total Particle Abundances*

179 The LISST detected on the order of 10^8 particles per liter at most stations through most of the
180 water column (Fig. 2). At most stations, there was an increase in particle abundance, usually to around
181 10^9 particles per liter, just above the floor of the Bay. In the anoxic water, particle abundance was
182 generally lower, often around 10^7 particles per liter. There were regions of apparently very low particle
183 numbers in the oxycline, in stations where an oxycline was present (Fig. 2). A general additive model
184 of form $\text{gam}(\text{Total_Particles} \sim s(\text{Pressure}) + s(\text{pressure, by} - \text{as.factor}(\text{Station})))$ indicated that across
185 all stations, this variability with depth was statistically detectable, and that there was statistically
186 significant station to station variability ($R^2 = 0.78$ (overall model), $p < 0.001$ (for all interaction terms
187 but one (pressure * station 3.3))). Particle abundance normalized to LISST size bins decreased as
188 particle size increased (Fig. 3).

189 *Particle Size to Abundance Relationship*

190 At all stations, there was a negative power law relationship between particle size and particle
191 abundance. The slope of the power law distribution, which is the slope of the relationship between log

192 transformed particle abundance and log transformed particle size, ranged at most stations and depths
193 from -3.5 to -4. However, several depths at some stations had anomalously large negative particle size
194 distribution slopes (Fig. 4). A general additive model $\text{gam}(\text{Particle_Size_Distribution_Slope} \sim$
195 $s(\text{Pressure}) + s(\text{pressure, by} - \text{as.factor}(\text{Station}))$), suggested that there was statistically significant
196 variability in the particle size distribution between depths, and that this relationship varied between
197 stations ($R^2 = 0.167, p < 0.01$).

198 *Total Particle Mass Patterns*

199 Estimated total particle mass per liter of all particles $> 1.2 \mu\text{m}$ ranged from 10 to 100 mg /L
200 (Fig. 5). Calculated particulate matter concentrations were higher in the bottom sample than the surface
201 sample at every station except 4.3 (OLS $\log(\text{Mass}) \sim \text{Depth} [\text{Surface or Bottom, excludes Oxycline}]$, F
202 $= 7.6, p = 0.02$). At station 4.3 the sample taken in the oxycline had highest biomass, followed by the
203 surface sample, and then the bottom sample. Particulate matter concentrations estimated by LISST
204 measurements were generally higher in the surface than in the bottom, except at stations 3.1 and 3.2.
205 There was no detectable relationship between station latitude and observed particle mass (Ordinary
206 Least Squares regression of form $\log(\text{Mass}) \sim \text{Latitude}$; $F = 0.001, p = 0.97$).

207 *Particle Mass to Size Relationship*

208 Mass per particle increased with particle size, following a power law (Fig. 6). The masses of
209 particles of each size class were similar at each depth, ranging from about 10^{-9} mg/particle in the 1.2
210 μm class to about 10^{-3} mg/particle in the 500 μm class. There did not appear to be statistically
211 significant differences between the slopes of the relationship between particle size and particle mass
212 (Fig. 6). A linear model of form $\ln(\text{Mass}) \sim \ln(\text{Size}) * \text{Station} * \text{Depth}$, where “ln” indicates the
213 natural logarithm function, found that while there was a relationship between size and mass ($p < 10^{-10}$),
214 neither station, depth, nor any interaction between size, station and or depth had any statistically
215 significant relationship to particle mass. However, a linear model of form $\ln(\text{Mass}) \sim \ln(\text{Size}) +$

216 Station` suggested that there was station to station variability in the intercept of the size to mass
217 relationship ($p < 0.01$ for all stations, with the exception of stations 3.2 and 3.1 which had statistically
218 identical intercepts). The `eemmeans` package was used to compare the y intercepts of the size to mass
219 relationship at each station. It was found that station 3.1 had statistically significantly lighter particles,
220 adjusted for size, than stations 4.3 (difference = -2.5 ± 0.7 (1 standard error) $\log(\text{mg/Particle})$, t-ratio =
221 -3.86 , $p = 0.012$) or 5.1 ($p = 2.5 \pm 0.7 \log(\text{mg/Particle})$, t-ratio = -3.79 , $p = 0.014$). All other
222 differences were found to be not statistically significant, after adjusting for multiple comparisons (FDR
223 < 0.05). (Fig. 7).

224 *Calculated Total Particle Mass Profiles*

225 By combining the information from the mean particle size to mass relationship with the
226 abundances of particles at each size, we were able to calculate expected particle mass throughout the
227 water column at each station (Fig. 5; black circles). A general additive model of form
228 `gam(Total_Particle_Mass ~ s(Pressure) + s(pressure, by = Station))` suggested that particle mass
229 varied statistically significantly between depths ($F = 9.4$, $p < 10^{-10}$), with all stations except 3.3 and 5.5
230 showing statistically significant deviations from the main profile ($F \geq 3.1$ $p < 0.003$ for all remaining
231 stations). Calculated total particle mass appeared to be related to, but was often an underestimate of,
232 observed total particle mass (Fig. 5).

233 **Discussion**

234 Measurements of physical and chemical parameters (Fig. 1) showed depth profiles typical of
235 previous measurements of the Chesapeake Bay at this time of year (Pritchard 1952; Murphy et al.
236 2011). The location of the stations arranged along the length of the Bay allowed for gradients to be
237 observed. The salinity gradient in the Chesapeake is formed as colder, denser saline water enters the
238 mouth of the Bay and flows northward, while warmer, less dense, freshwater enters from rivers and
239 tributaries and moves south (Pritchard 1952). The density difference in these two layers forms a

240 pycnocline, which was observed at all stations. The pycnocline blocks the vertical transfer of oxygen,
241 creating the anoxic zones that were seen in most stations. Large anoxic and hypoxic zones form during
242 summer in the Chesapeake Bay and were clearly seen in July when measurements were taken. Anoxic
243 bottom waters have been shown to lead to increases in sulfide concentrations (Roden and Tuttle 1992),
244 as seen in the sulfidic samples collected in stations 4.3 and 5.1.

245 Throughout the Chesapeake Bay, particle size distribution profiles displayed a power law
246 relationship between size and abundance, with slope usually between -3.5 and -4, which is within the
247 range of values seen in open ocean locations (Sheldon et al. 1972; Kostadinov et al. 2009; Cram et al.
248 2018). The slopes generally did not show much change with depth. This pattern is consistent with the
249 findings of a study that size distribution does not change significantly with depth across the Atlantic
250 Ocean (Gordon 1970), though it contrasts with measurements of an oxygen deficient zone in the
251 Eastern Tropical North Pacific that found changes in the particle size slope with depth (Cram et al.
252 2021). While particle size spectra have been measured in the Chesapeake Bay, the particle size
253 distribution slope is often not reported (Schubel 1968; Schubel and Nelson 1973). The anomalous
254 spikes of particularly negative slopes, seen especially in stations 4.3, 5.1, and 5.5, could indicate a lack
255 of large particles in the oxycline, as the spikes occurred at approximately the same depth. These spikes
256 could also be artifacts, perhaps induced by changes in salinity or temperature or introduced by the
257 LISST's electronics.

258 The particle size to mass relationship also stayed consistent throughout stations and depths,
259 with mass increasing and density decreasing in larger particles. The slopes of the size to mass
260 relationship, or fractal dimension, at each station and sample depth were similar to the values
261 calculated in other particle studies. For instance, Fall et al. (2021) calculated fractal dimension in the
262 York River as the size to density relationship with a bulk value of 2.25. Other studies have quantified
263 fractal dimensions from the size to density or size to settling velocity relationship in the Chesapeake

264 Bay (Sanford et al. 2004) and other estuaries and marine environments (Hill et al. 1998; Guidi et al.
265 2008; Jackson et al. 1997). These previous measurements of fractal dimension values for particles
266 typically fall somewhere between 1.3 and 2.5, and the values for this study are on the low end of that
267 range. Aggregation and disaggregation of particles affect their fractal dimension, with larger aggregates
268 having lower fractal dimensions than small particles. Li and Logan (1995) found fractal dimension to
269 decrease from 2.49 to 1.68 as particles coagulated during a phytoplankton bloom. It is possible that
270 collection methods in this study could lead to disaggregation of particles; however, the fractal
271 dimensions' consistency with other studies lend confidence to our observations.

272 Although particle size to mass relationships stayed consistent across stations and depth, total
273 particle abundance and mass both varied by depth. Particle abundance profiles generally tracked total
274 particle mass profiles (Fig. 2 and 5). The calculated total mass values from collected particles were
275 consistently higher than the estimated mass based on LISST measurements, especially in station 4.3
276 (Fig. 5). This disparity could be caused by the assumption that the power law relationship between size
277 and mass is the same at each station. Particle abundance and total particle mass both increased near the
278 bottom of the water column, suggesting that the current is resuspending sediment from the floor of the
279 Bay. In the anoxic water below the pycnocline, particle abundance and total mass was lower than in
280 surface waters, suggesting either lower production of particles in this region or faster removal. This
281 effect may occur when the pycnocline separates anoxic water from the more productive surface waters,
282 which prevents particles that primarily form in the surface from mixing into the anoxic waters. This
283 scarcity of particle mass below the pycnocline suggests either low transport or fast removal of particles
284 into this region. We argue that since particle remineralization is thought to be slow in anoxic water
285 (Cram et al. 2018), it is likely the former process, low *in situ* production and low flux from the surface
286 that leads to the lower anoxic particle mass. Particle abundance and particle mass profiles diverged near
287 the middle of the depth profiles, where abundance sharply decreased in most stations, but mass did not.

288 This result could suggest that the decreases in particle abundance were generally among small particles
289 that had less impact on biomass, although the size distribution slopes in some stations suggest that
290 small particles were still more abundant relative to large particles in the oxycline. The sharp decreases
291 in particle abundance could also be the same artifacts that may be seen in the particle distribution
292 slopes.

293 This study was the first characterization of particle size to abundance and size to mass
294 distribution across the length of the Chesapeake Bay as well as with depth. Overall, there was little
295 variation by latitude, with particle size, abundance, and mass mostly following the same patterns at
296 each station. Although the Bay covers a large area and sample stations varied in proximity to the
297 Susquehanna River and the mouth of the Bay, the results suggest that factors other than latitude lead to
298 a variability of particle characteristics. Significant differences were observed vertically, with particle
299 mass and abundance higher just above the floor and low in the body of the anoxic layer. This low total
300 particle mass in the anoxic water suggests that particles from the photic zone are not mixing into the
301 anoxic water, and also that particle sinking flux happens on either a slower or similar time scale to
302 carbon removal, either by carbon settling into the sediment or by remineralization. The low particle
303 abundances could indicate the presence of particle remineralization despite the lack of oxygen, because
304 if remineralization was absent, we would expect carbon accumulation in this region even if particle flux
305 into the region was low. The mass of particles also suggests low input of carbon into this region,
306 suggesting carbon limitation of microorganisms in the anoxic region.

307 **Conclusion**

308 This analysis of particulate organic matter provides data for particle size distribution and
309 particle mass at surface and bottom depths across various stations in the mesohaline region of the
310 Chesapeake Bay. This study was the first to analyze particle distribution at multiple locations in the
311 Bay, with samples collected at the same time. Generally, particle size/abundance and size/mass

312 relationships were similar between stations and depths. Particle abundance and mass mostly followed
313 similar patterns to each other, decreasing in the anoxic zones, with an increase near the bottom of the
314 Bay. The results show the influence of depth on particle distribution, while patterns stayed consistent
315 throughout station latitudes at the time of sample collection in July.

316

317

318

319

320

321

322

323

324

325

326

327

328

329

330

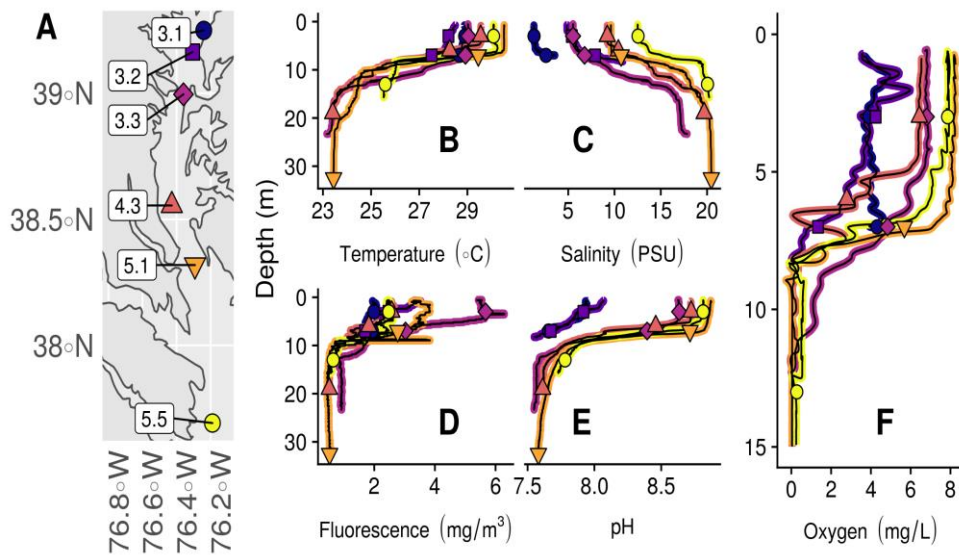
331

332

333

334

335



336

337 **Fig. 1** Sample Collection locations (A) and corresponding oceanographic data (B-F) measured by a
 338 seabird CTD. These included Temperature (A), Salinity (B), Fluorescence (D), pH (E), and oxygen (F).
 339 Shapes in the CTD profiles indicate the locations where particle samples were collected. Lines indicate
 340 the corresponding CTD profiles. All stations have two samples, one in the upper mixed layer, and one
 341 below, except station 4.3 which also has a sample taken at the oxycline. CTD profiles all extend from
 342 the surface to approximately 5 m above the seafloor, except station 5.5, which only extended to 15 m

343

344

345

346

347

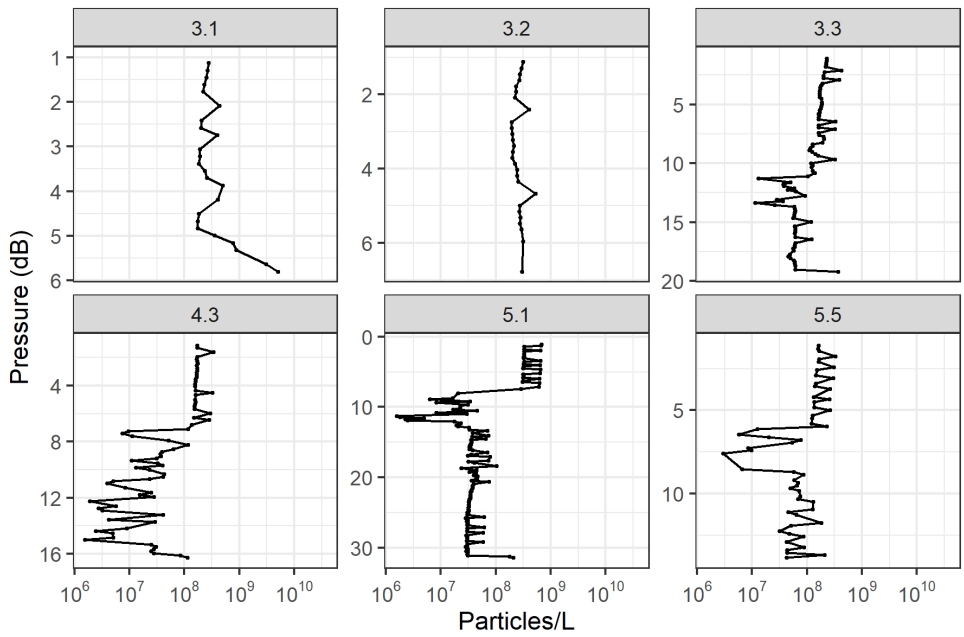
348

349

350

351

352



353

354 **Fig. 2** Particle Abundance. The number of particles per liter of water throughout the water column, as
 355 estimated by the LISST. The y axis indicates pressure in dB. The x axis is on a log scale and indicates
 356 total particles per liter

357

358

359

360

361

362

363

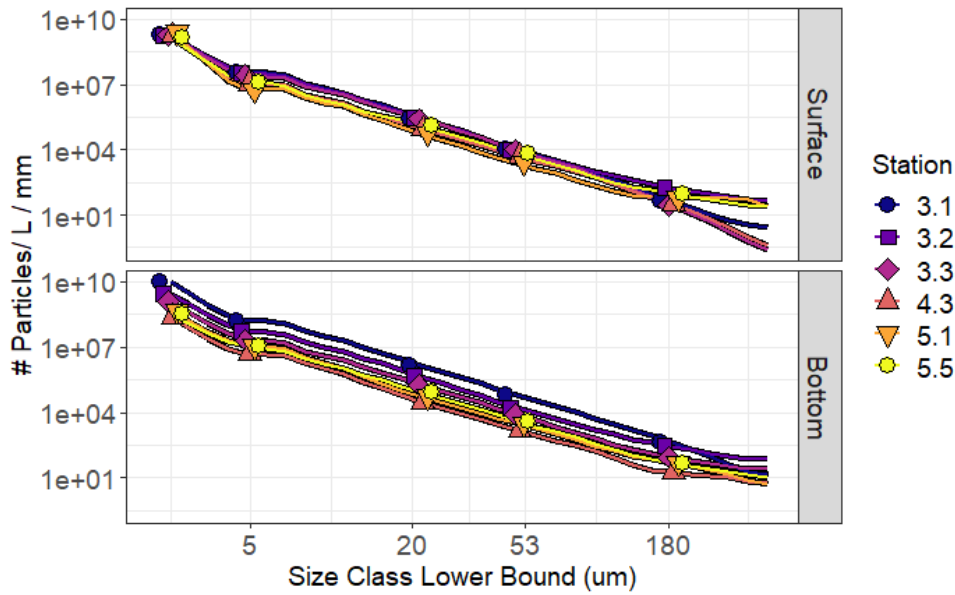
364

365

366

367

368



369

370 **Fig. 3** Particle Abundance at Sample Depths. The number of particles per liter of water per particle size
 371 (x axis) for all size bins provided by the LISST (y axis), shown only for the surface and bottom depths
 372 where particle samples were collected. Points are where the LISST size bins most closely match the
 373 sizes of the filters that were used for particle collection

374

375

376

377

378

379

380

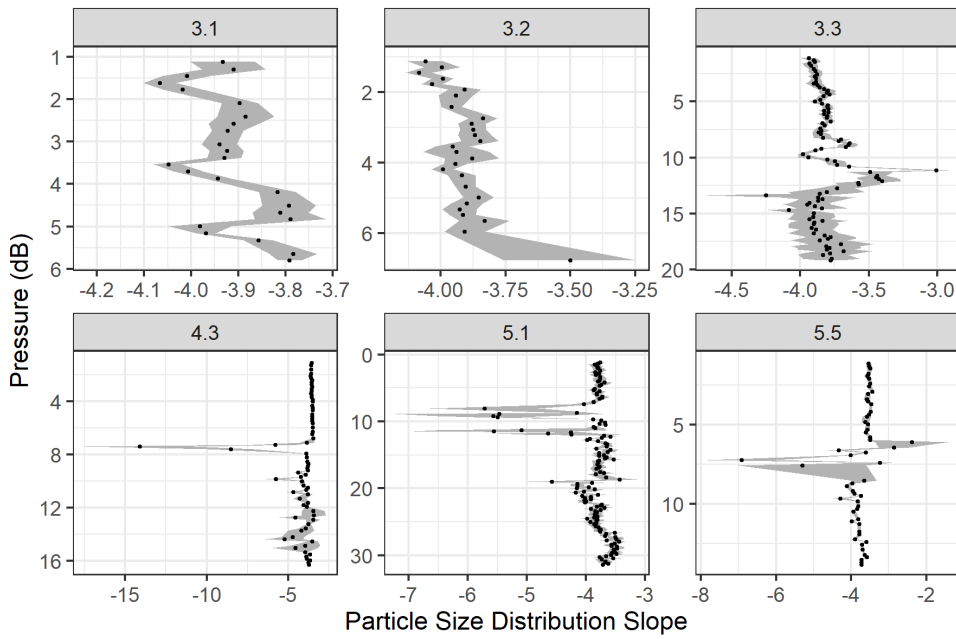
381

382

383

384

385



386

387 **Fig. 4** Particle size distribution slopes (x axis) indicate the slope of the relationship between log
 388 transformed particle size and log transformed particle abundance. More negative values indicate a
 389 higher relative proportion of small particles and a smaller relative proportion of large particles

390

391

392

393

394

395

396

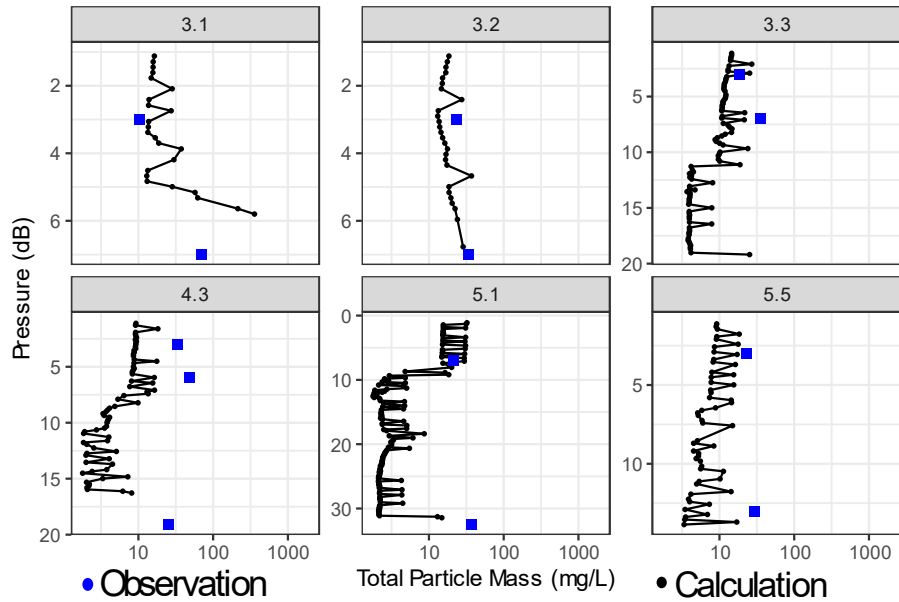
397

398

399

400

401



402

403 **Fig. 5** Blue squares – Total particle mass collated at each station. Total Observed Particulate mass was
 404 determined by summing over all size fractions and includes both organic and inorganic matter. Black
 405 circles – Total calculated particle mass was estimated by multiplying LISST measurements of size
 406 specific particle abundances by size specific particle mass estimates

407

408

409

410

411

412

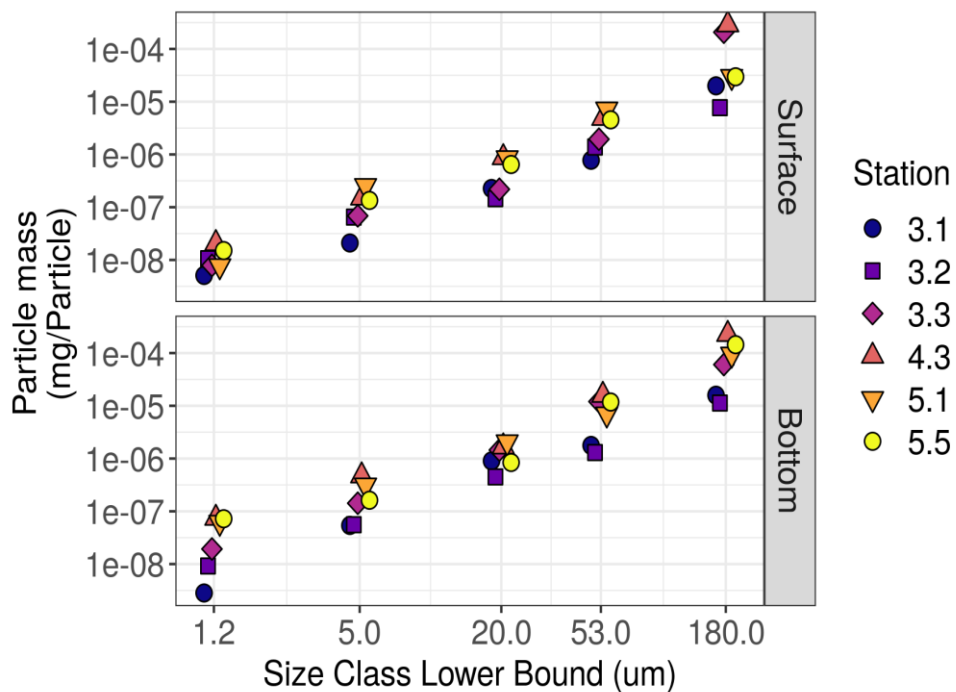
413

414

415

416

417



418

419 **Fig. 6** Mass per Particle. The mass of the total particles collected on each size filter normalized to
 420 particle abundance. Mass was calculated for each particle size using the diameters on the lower bound
 421 of each size bin. These results are virtually the same as when calculated with the geometric mean of
 422 each bin, suggesting that most particles are on the low end of their bin size range

423

424

425

426

427

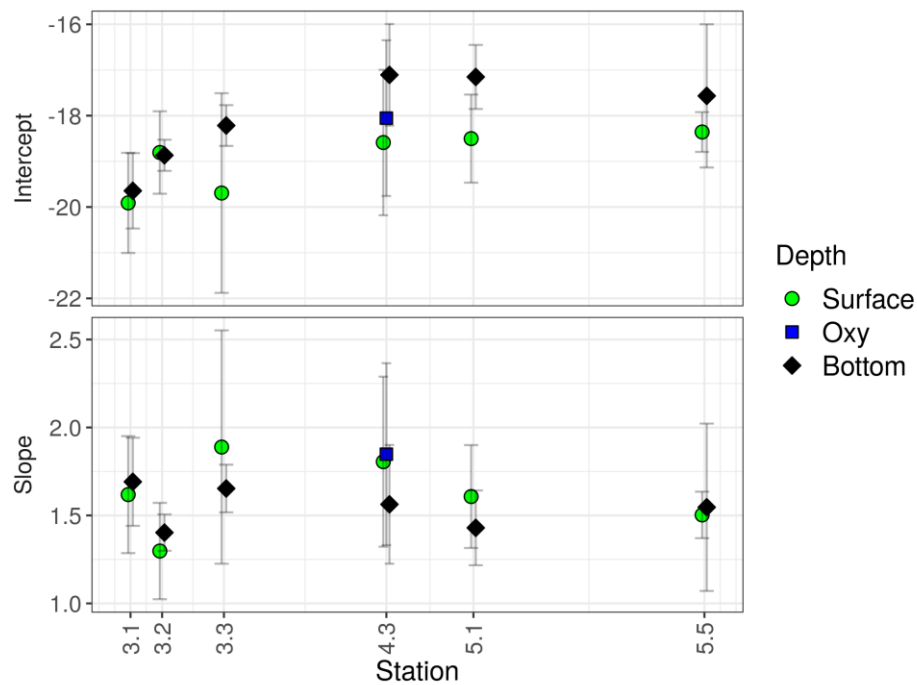
428

429

430

431

432



433

434 **Fig. 7** The intercepts (natural log of the predicted mass of particles 1 μm in size) and slope of the mass

435 to size relationship depicted in Figure 6. Confidence intervals indicate 2 standard errors

436

437

438

439

440

441

442

443

444

445

446

447

448 **References**

- 449 Biggs, R.B. 1969. Sources and distribution of suspended sediment in northern Chesapeake Bay. *Marine*
450 *Geology*. 9: 187-201.
- 451 Canuel, E.A. and A.R. Zimmerman. 1999. Composition of particulate organic matter in the southern
452 Chesapeake Bay: sources and reactivity. *Estuaries*. 22(4): 980-994.
- 453 Chen S., D. Eisma, and J. Kalf. 1994. In situ size distribution of suspended matter during the tidal cycle
454 in the Elbe Estuary. *Netherlands Journal of Sea Research*. 32(1): 37-48.
- 455 Cram J., C. Fuchsman, M. Duffy, J. Pretty, R. Lekanoff, J. Neibauer, et al. 2021. Slow particle
456 remineralization, rather than suppressed disaggregation, drives efficient flux transfer through
457 the Eastern Tropical North Pacific Oxygen Deficient Zone (preprint). *Oceanography*.
- 458 Cram, J.A., T. Weber, S.W. Leung, A.M.P. McDonnell, J.H. Liang, C. Deutsch. 2018. The role of
459 particle size, ballast, temperature, and oxygen in the sinking flux to the deep sea. *Global*
460 *Biogeochemical Cycles*. 32: 858-876.
- 461 Eisma, D. 1991. Particle size of suspended matter in estuaries. *Geo-Marine Letters*. 11(3): 147-153.
- 462 Fall K.A., C.T. Friedrichs, G.M. Massey, D.G. Bowers, and S.J. Smith. 2021. The importance of
463 organic content to fractal floc properties in estuarine surface waters: Insights from video,
464 LISST, and pump sampling. *Journal of Geophysical Research: Oceans*. 126. e2020JC016787.
- 465 Fisher T.R., J.D. Hagy, and E. Rochelle-Newall. 1998. Dissolved and particulate organic carbon in
466 Chesapeake Bay. *Estuaries*. 21(2): 215.
- 467 Fugate, D.C. and C.T. Friedrichs. 2002. Determining concentration and fall velocity of estuarine
468 particle populations using ADV, OBS, and LISST. *Continental Shelf Research*. 22: 1867-1886.
- 469 Fugate, D.C. and C.T. Friedrichs. 2003. Controls on suspended aggregate size in partially mixed
470 estuaries. *Estuarine, Coastal and Shelf Science*. 58(2): 389-404.

471 Gordon, D.C. 1970. A microscopic study of organic particles in the North Atlantic Ocean. *Deep-Sea*
472 *Research*. 17: 175-185.

473 Guidi L., G.A. Jackson, L. Stemann, J.C. Miquel, M. Picheral, and G. Gorsky. 2008. Relationship
474 between particle size distribution and flux in the mesopelagic zone. *Deep-Sea Research I*. 55:
475 1364-1374.

476 Hill P.S., J.P. Syvitski, E.A. Cowan, and R.D. Powell. 1998. In situ observations of flocc settling
477 velocities in Glacier Bay, Alaska. *Marine Geology*. 145: 85-94.

478 Hill P.S., G. Voulgaris, and J.H. Trowbridge. 2001. Controls on flocc size in a continental shelf bottom
479 layer. *Journal of Geophysical Research*. 106(C5): 9543-9549.

480 Jackson G.A., R. Maffione, D.K. Costello, A.L. Alldredge, B.E. Logan, and H.G. Dam. 1997. Particle
481 size spectra between 1 μm and 1 cm at Monterey Bay determined using multiple instruments.
482 *Deep Sea Research Part I: Oceanographic Research Papers*. 44(11): 1739–1767.

483 Jonas, R.B. 1992. Microbial processes, organic matter and oxygen demand in the water column, p. 113-
484 148. In D. E. Smith, M. Leffler, and G. Mackiernan (eds.), *Oxygen Dynamics in the*
485 *Chesapeake Bay: A Synthesis of Recent Research*. Maryland Sea Grant, College Park,
486 Maryland.

487 Jonas, R.B. and J.H. Tuttle. 1990. Bacterioplankton and organic carbon dynamics in the lower
488 mesohaline Chesapeake Bay. *Appl. Environ. Microbiol.* 56(3): 747-757.

489 Kemp W., P. Sampou, J. Garber, J. Tuttle, and W. Boynton. 1992. Seasonal depletion of oxygen from
490 bottom waters of Chesapeake Bay: roles of benthic and planktonic respiration and physical
491 exchange processes. *Marine Ecology Progress Series*. 85: 137–152.

492 Kostadinov T.S., D.A. Siegel, and S. Maritorena. 2009. Retrieval of the particle size distribution from
493 satellite ocean color observations. *Journal of Geophysical Research (Oceans)*. 114: C09015.

494 LISST-100X Particle Size Analyzer User's Manual. 2015. *Sequoia Scientific, Inc.* Version 5.1.

495 Li, X. and B.E. Logan. 1995. Size distributions and fractal properties of particles during a simulated
496 phytoplankton bloom in a mesocosm. *Deep Sea Research Part II: Topical Studies in*
497 *Oceanography*. 42(1): 125-138.

498 Loh A.N., J.E. Bauer, and E.A. Canuel. 2006. Dissolved and particulate organic matter source-age
499 characterization in the upper and lower Chesapeake Bay: a combined isotope and biochemical
500 approach. *Limnology and Oceanography*. 51(3): 1421-1431.

501 Middelburg, J.J. and P.M.J Herman. 2007. Organic matter processing in tidal estuaries. *Marine*
502 *Chemistry*. 106(1-2): 127-147.

503 Murphy R.R., W.M. Kemp, and W.P. Ball. 2011. Long-Term Trends in Chesapeake Bay Seasonal
504 Hypoxia, Stratification, and Nutrient Loading. *Estuaries and Coasts*. 34: 1293-1309.

505 Officer C.B., R.B. Biggs, J.L. Taft, L.E. Cronin, M.A. Tyler, and W.R. Boynton. 1984. Chesapeake Bay
506 anoxia: origin, development, significance. *Science*. 223: 22-27.

507 Pritchard, D.W. 1952. Salinity distribution and circulation in the Chesapeake Bay estuarine system.
508 *Journal of Marine Research*. 11: 106-123.

509 R Core Team. 2019. R: A language and environment for statistical computing. R Foundation for
510 Statistical Computing, Vienna, Austria. URL <https://www.R-project.org/>.

511 Rasse, R. and G. Dall’Olmo. 2019. Do Oceanic Hypoxic Regions Act as Barriers for Sinking Particles?
512 A Case Study in the Eastern Tropical North Atlantic. *Global Biogeochemical Cycles*. 33(12):
513 1611-1630.

514 Robinson, C. 2019. Microbial Respiration, the Engine of Ocean Deoxygenation. *Frontiers in Marine*
515 *Science*. 5: 533.

516 Roden, E.E. and J.H. Tuttle. 1992. Sulfide release from estuarine sediments underlying anoxic bottom
517 water. *Limnology and Oceanography*. 37: 725–738.

518 Sanford L.P., P.J. Dickhudt, L. Rubiano-Gomez, M. Yates, S.E. Suttles, C.T. Friedrichs, D.D. Fugate,
519 and H. Romine. 2004. Variability of Suspended Particle Concentrations, Sizes, and Settling
520 Velocities in the Chesapeake Bay Turbidity Maximum. In *Flocculation in Natural and*
521 *Engineered Environmental Systems*, ed. I.G. Droppo, G.G. Leppard, S.N. Liss, and T.G.
522 Milligan, 211-236. Boca Raton: CRC Press.

523 Sanford L.P., S.E. Suttles, and J.P. Halka. 2001. Reconsidering the physics of the Chesapeake Bay
524 estuarine turbidity maximum. *Estuaries*. 24(5): 655–669.

525 Savoye N., V. David, F. Morisseau, H. Etcheber, G. Abril, I. Billy, K. Charlier, G. Oggian, H.
526 Derriennic, and B. Sautour. 2011. Origin and composition of particulate organic matter in a
527 macrotidal turbid estuary: The Gironde Estuary, France. *Estuarine, Coastal and Shelf Science*.
528 108(2012): 16-28.

529 Sheldon R.W., A. Prakash, and W.H. Sutcliffe. 1972. The size distribution of particles in the ocean.
530 *Limnology and Oceanography*. 27(3): 327-340.

531 Schubel, J.R. 1968. Turbidity maximum of the northern Chesapeake Bay. *Science*. 161(3845): 1013–
532 1015.

533 Schubel, J.R. and R.B. Biggs. 1969. Distribution of seston in upper Chesapeake Bay. *Chesapeake*
534 *Science*. 10(1): 18-23.

535 Schubel, J.R. and B.W. Nelson. 1973. Distribution and Transportation of Suspended Sediment in the
536 Upper Chesapeake Bay. In Environmental Framework of Coastal Plain Estuaries. *Geological*
537 *Society of America Memoirs*. 133: 151-167.

538 Schubel, J.R. and D.W. Pritchard. 1986. Responses of upper Chesapeake Bay to variations in discharge
539 of the Susquehanna River. *Estuaries*. 9: 236-249.

540 Testa, J.M., W.M. Kemp, and W.R. Boynton. 2018. Season-specific trends and linkages of nitrogen and
541 oxygen cycles in Chesapeake Bay. *Limnology and Oceanography*. 63: 2045-2064.

542 Wang, J. and R.R. Hood. 2021. Modeling the Origin of the Particulate Organic Matter Flux to the
543 Hypoxic Zone of Chesapeake Bay in Early Summer. *Estuaries and Coasts*. 44: 672-688.